Research Square

Preprints are preliminary reports that have not undergone peer review.
They should not be considered conclusive, used to inform clinical practice,
or referenced by the media as validated information.

Thermo-regulatory response of static and dynamic breast thermography as a biomarker of malignancy

Meir Gershenson

meir.gershenson@gmail.com

Article

Keywords: Breast cancer, dynamic thermogram, independent component analysis, static thermogram, tumor heat, vasomodulation, unsupervised training

Posted Date: November 6th, 2026

DOI: https://doi.org/10.21203/rs.3.rs-10895336/v1

License: This work is licensed under a Creative Commons Attribution 4.0 International License.
Read Full License

Additional Declarations: No competing interests reported.

Thermo-regulatory response of static and dynamic breast thermography as a biomarker of malignancy.

Meir Gershenson

Independent researcher, Laurel 134, Cholul, Mérida, México 97305, meir.gershenson@gmail.com.

Abstract

This study assesses the diagnostic potential of static and dynamic infrared thermography by relating physiological vascular patterns to established indicators of breast malignancy. Mammography remains the principal global screening modality; however, its accuracy declines in women with dense breast tissue [1], and its high cost limits access in developing countries [2]. Although dynamic thermal imaging may improve lesion detection, its clinical implementation in developing settings is constrained by the opacity of artificial intelligence models and the limited availability of high-quality datasets [3]. This paper presents a physiology-based model intended to reduce reliance on extensive training data and thereby facilitate analysis in small patient cohorts. Earlier Virtual Wave Transformation approaches appear to capture dynamic thermal responses but struggle to differentiate metabolic heat from vascular signals. The present study combines dynamic thermal imaging with static infrared imaging. By exploiting the different temporal behaviors of these signals, the model may distinguish increased cancer-related metabolic activity from other thermal patterns.

In contrast to black-box deep-learning systems and even explainable AI approaches, this algorithm provides a more interpretable mathematical alternative by decomposing thermal patterns and separating convective vascular heat transport from thermal conductive metabolic signals. Analysis of the temporal variation in each component's amplitude indicates a possible association with patient diagnosis. Whereas conventional AI methods generally require large databases and expensive clinical validation, such as MRI, this approach uses physiological parameters to obtain diagnostic information from smaller samples. This work is a limited pilot study focused on evaluating the mathematical methods; we did not perform detailed statistical analysis.

Keywords: Breast cancer; dynamic thermogram; independent component analysis; static thermogram; tumor heat; vasomodulation; unsupervised training.

1. Introduction

Breast cancer remains a leading cause of cancer-related mortality, and its burden falls disproportionately on resource-constrained settings because of late-stage presentation and limited access to affordable screening [4]. Mammography, the clinical standard, loses sensitivity in dense breast tissue, motivating complementary physiological modalities [5, 6]. Dynamic infrared thermography, which monitors the breast's thermal recovery after a stimulus, may reveal abnormal perfusion with improved sensitivity [7, 8]. However, vascular responses alone have historically proved insufficient for cancer detection: the vascular system transports much of the tumor-derived heat, obscuring the conductive signal from tissue to skin. Distinguishing pathological metabolic heat from normal thermal variability—including benign elevations from inflammation and hormonal changes [9,10] therefore requires precise characterization of breast-tissue heat signatures.

Existing computational approaches do not meet this need. AI-based methods require extensive labeled datasets, risk overfitting, and function as black boxes, leaving clinicians without causal transparency [11, 12]; only one AI system has reached clinical use, and most focus on static images. Inverse modeling has been applied only to static distributions, where superficial neovascularization can obscure the tumor's heat signal. Matrix-factorization and Virtual Wave Transformation approaches, drawn from thermal nondestructive evaluation, resolve diffusion-related effects but overlook slowly varying, static metabolic signatures [13, 14]. Data constraints compound these limits: with detection in only 5.1 cases per 1,000 screenings, meaningful validation requires large cohorts and costly MRI; only two large FDA-registered studies appear to have been completed. The primary public dataset is small and substantially inconsistent [15].

Here we address these limitations with a physiology-based decomposition of dynamic thermal imaging. By applying independent component analysis to the static frame and 20 DTI frames, we separate the mixed thermal signal into statistically independent components and classify transient vascular patterns. Because the method is anchored in physiology and heat-transport mechanisms rather than data-intensive training, it yields

an interpretable biomarker of malignancy that remains effective for small cohorts without expensive, large-scale validation.

.

2. Method

A virtual wave transform (VWT) thermography study [5] analyzed skin DTI data after external cooling, isolated vascular and active physiological heat signatures, but failed to identify a heat signature dependent on cancer presence. This analysis included all patients not excluded for excessive motion, regardless of whether the affected breast was specified as left or right. A lack of well-characterized patients may limit AI studies; this study performed very well despite limited training data. Each image is converted into a single vector $\boldsymbol{V}$. Using independent component analysis (ICA), the thermal data are decomposed into principal components $\boldsymbol{W}$ and a temporal matrix $\boldsymbol{H}$. ICA assumes statistical independence between tumor heat generation and vascular blood flow. However, physiological literature indicates that tumor-induced angiogenesis and metabolic heat generation are coupled. These sources are not truly independent; consequently, ICA may produce mixed components. The dependence indicates a common source with different mechanisms. To separate vascular heat, the analysis uses the temporal information in matrix $\boldsymbol{H}$. The ICA algorithm may be computationally inefficient because it relies on a random search. Principal component analysis (PCA) may be more efficient as it has an analytical implementation. The authors used PCA factorization as an initial approximation for ICA. The algorithm had two steps: first, the authors performed ICA on the 21 images (20 dynamic and one static) to generate the matrices $\boldsymbol{H}$ and $\boldsymbol{W}$; then, we analyzed the ensemble to obtain statistical indicators of malignancy. Because of data quality limitations, the authors consider this a pilot study testing mathematical tools; they did not elaborate on statistical evaluation, which should be done in future studies. Figure 1 presents a block diagram of the algorithm.

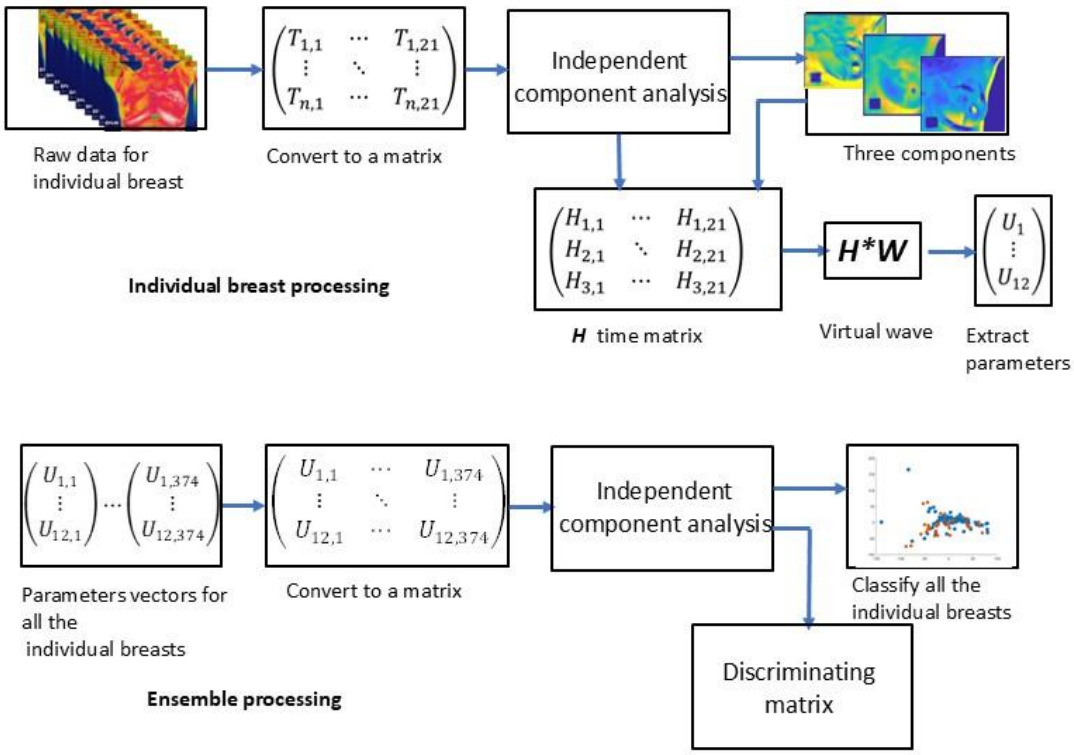


Fig. 1. Block diagram of data processing. The workflow illustrates the transition from raw infrared sequence acquisition to extracting independent component maps, which are then processed to identify thermal markers indicative of malignancy.

2.2. Data

The dataset consists of infrared sequences acquired from patients undergoing a standardized cold-stress protocol [15], capturing temporal thermal variations over a defined recovery interval. The experimental dataset comprises infrared thermographic sequences from 287 patients, including both healthy individuals and patients with confirmed breast malignancies. Although this database has been widely used, particularly in recent artificial intelligence studies, it may have significant limitations, as discussed in Appendix I. In particular, only four patients had tumors localized to a specific breast quadrant and side of the body, limiting the study's generalizability and restricting its findings to preliminary results. Consequently, future research may need to

prioritize acquiring larger, more diverse clinical datasets to validate the robustness of these thermal markers across different patient populations. We analyzed each breast as an independent case; however, ambiguity regarding laterality remains a significant limitation. The method's robustness, as samples categorized as healthy or pathological are optional, mitigates this limitation. We obtained dynamic thermographic image sequences by cooling patients' skin with a fan until it reached 32.5°C or 5 minutes had elapsed, whichever occurred first, then recorded thermal images every 15 seconds for an additional 5 minutes. The ambiguity in the cooling period introduced several challenges during virtual-wave processing, as we lacked the true cooling duration. We used 3 minutes of cooling as the default.

2.3. Data screening

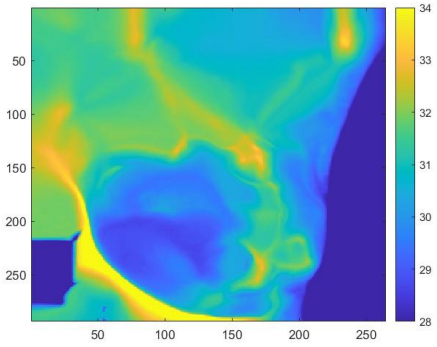
Apparent breast deformities and inter-frame registration failures were excluded. In addition to the dynamic images, we included a static thermogram; because it was captured at a different time, it may not have registered. Appendix II provides the registration algorithm. We rejected patients who failed registration. The dataset had a substantial limitation: approximately 25 patients had their static frame replaced mistakenly by the first dynamic frame. Data for those patients were rejected. Our algorithm identified this discrepancy only late in the study. Our reduced dataset comprised 119 individual breasts from healthy participants and 82 individual breasts from participants for whom at least one breast was classified as diseased, yielding 201 breasts from the original 287 patients. Among the 110 original patients classified as diseased, only 4 had documented malignancy locations; the remaining patients lacked documentation of the lesion's precise site. As a result, we consider this study preliminary, validating the methodology rather than drawing a medical conclusion.

3 Analysis

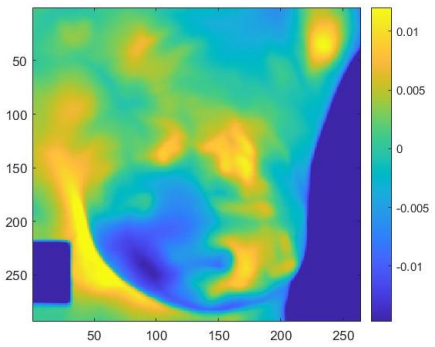
3.1. ICA Image Analysis

Unlike previous work, we included the static frame as the 21st frame and incorporated it into the factorization. After image registration, we subtracted 30°C from all frames, then converted each frame into a single column V. Stacking the columns for each patient yielded two matrices: one containing only the region of interest (the breast) and another containing the entire frame around the breast. For analysis, we used a matrix of image vectors comprising the region of interest (ROI) limited to the breast alone, and applied the results for display

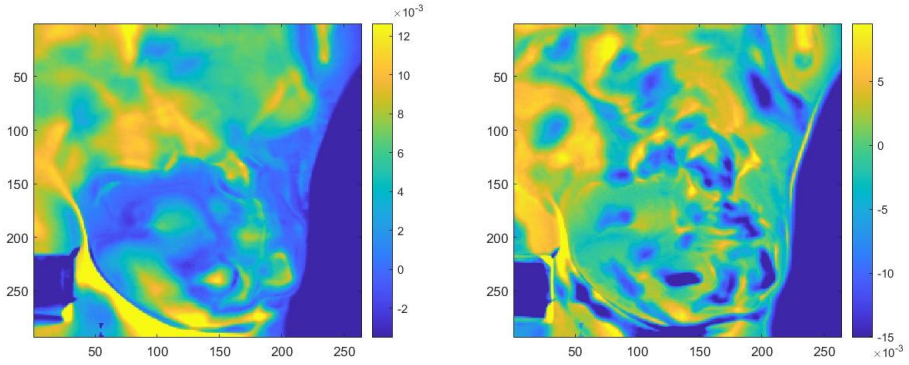
to the second matrix, which included the surrounding frame. Before matrix factorization, we applied a low-pass filter comprising a virtual wave, both forward and inverse. Appendix 3 details the filter construction. For each image group, we first applied principal component analysis (PCA), followed by independent component analysis (ICA). Although independent component analysis (ICA) was the primary objective, the PCA results were very similar to those of ICA and retained the advantage of an analytical implementation; unlike ICA, which requires a random search, PCA results are ordered by significance, which is useful in the analysis. ICA produces a factorization into two matrices: one temporal and one spatial. The convention is to normalize the first temporal matrix and fix its mean to be positive. We normalized the image matrix to a norm of one, multiplied the time matrix by the normalization factor to preserve the product of the two matrices, and kept the first matrix's polarity. Figure 1 shows a block diagram under "individual breast processing." Figures 2 and 3 present results for patient T0016, who was categorized as healthy. Figure 2a shows the static image, while Figures 2b–d show the three component images. The first component, representing the vascular system, resembles the static frame. The other two components appear substantially smaller in magnitude. Figure 3 shows the matrix $\boldsymbol{H}$. The first 20 points correspond to the dynamic data, and the 21st point corresponds to the static frame. The second component appears significant only at the static frame.



a



b



c **d**

Figure 2: Patient T016, healthy left breast: (a) static thermogram; (b) first component; (c) second component; (d) third component.

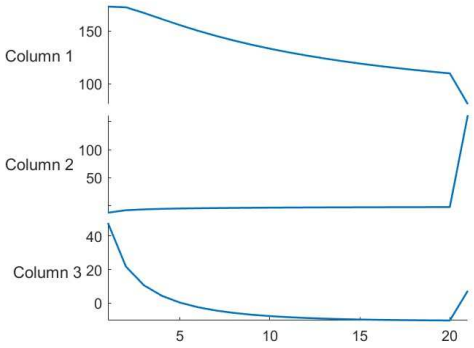
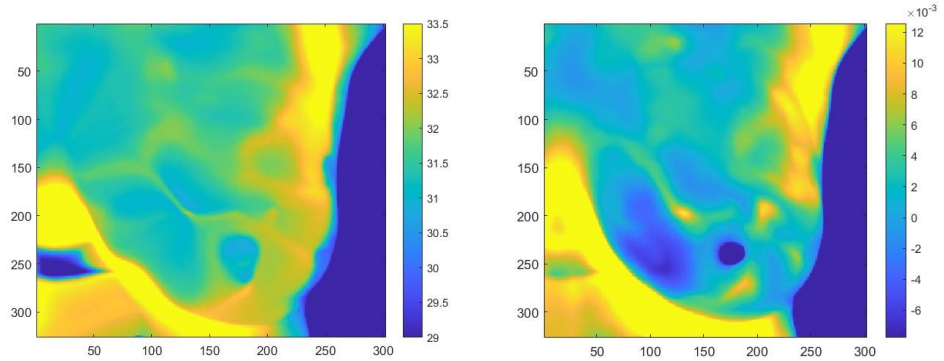
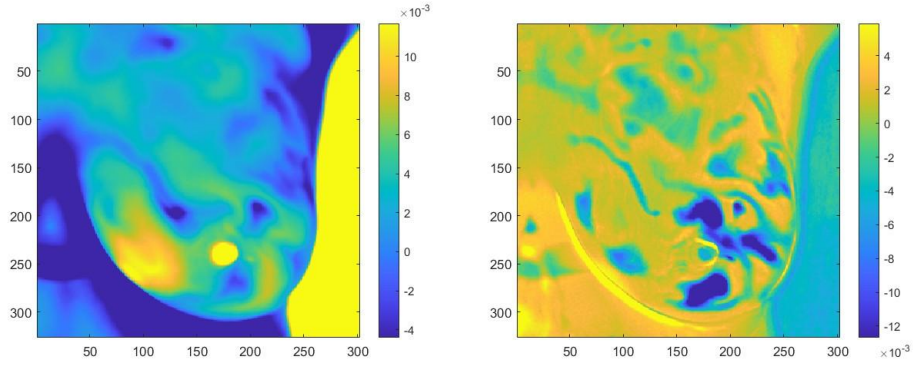


Figure 3: Time matrix ***H*** for patient T061's healthy left breast. Each trace corresponds to one image. Points 1–20 represent the dynamic amplitudes, whereas point 21 represents the static amplitude taken separately.



a **b**



C **d**

Figure 4. Patient T285 "sick": (a) static thermogram; (b) First component; (c) Second component; (d) Third component. Points 1–20 represent the dynamic amplitudes, whereas the 21st point represents the static amplitude. Amplitudes are based on normalization to one of each of the corresponding images. Unlike Figure 2c, Figure 2b shows a large, diffuse hot region, which corresponds to the diagnosis: the lower, medial left breast.

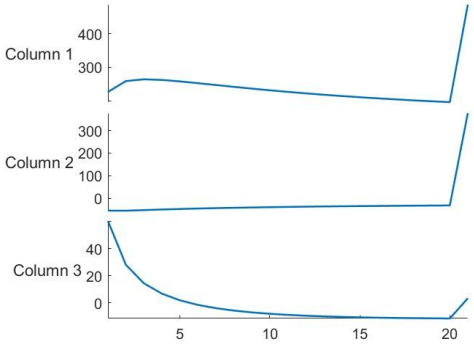
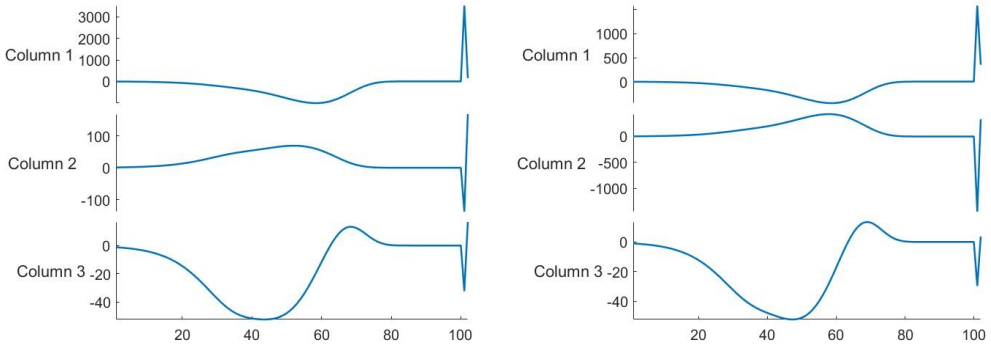


Figure 5. Time matrix of Patient T285's left breast ***H***. Each trace corresponds to one image. Points 1–20 represent the dynamic amplitudes, and the 21st is the static amplitude.

3.3. Virtual Wave Analysis

In the previous section, we analyzed the three components of the image matrix $\boldsymbol{W}$. In this section, we develop tools to analyze the time matrix $\boldsymbol{H}$. This adjustment preserves the physical scale of the thermal

responses, thereby permitting characterization of the distinct physiological behaviors of healthy and malignant tissue. The traces in Figures 3 and 5 may depict the temporal profiles encoded in matrix $\boldsymbol{H}$. The traces appear broadly similar across healthy and malignant cases, although a limited number of cases may exhibit divergent behavior.A virtual wave transform enhances time resolution. The transformation identifies reflections within the tissue by converting diffusive heat propagation into a virtual wave in which the time is proportional to distance, thereby isolating vascular signatures from background. Although virtual waves may resemble real waves, their resolution is limited by the ill-posed inversion of the matrix $\boldsymbol{W}$. We used the modified truncated eigenvalue inversion described in Appendix 3. By identifying reflections that exhibit the polarity of the applied thermal stimulus as vasoconstriction and reverse polarity at twice the depth as thermal reflection from high-conductivity vasculature. This enables resolution of subsurface thermal features otherwise masked by thermal propagation characteristics. Figures 6a and 6 b illustrate these resolved features.



a Patient T016, healthy left breast. **b** Patient T0285, sick left breast.

Figure 6 displays the virtual wave profile on a log scale; each10 points are multiples of 2. The 101st point is the offset value of the original dynamic frames recovered by the modified VWT, and point 102 corresponds to the static frame.

Thermograms of patients with disease and healthy individuals appear similar; only a small proportion of patients differ substantially. The first trace appears largely as constant (data point 101st), with slight cooling that indicates vasoconstriction. Its amplitude appears small in the static frame. The second trace shows a positive dynamic value, indicating thermal reflection from vasculature. The third trace, with a smaller magnitude, shows more pronounced early negative vasoconstriction and a smaller positive thermal-reflection

component. These distinct trace patterns reflect the method's capacity to isolate physiological responses related to vascular modulation.

3.4 Ensemble Analysis

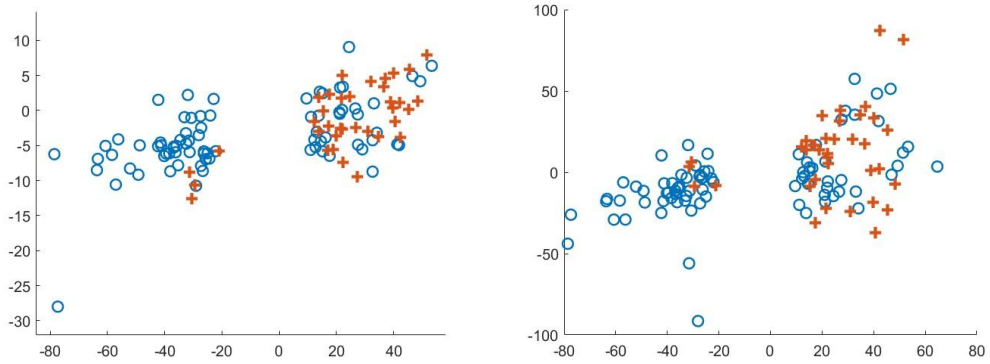
We repeated independent component analysis for all data from patients who passed the initial screening: 32 patients with disease and 82 healthy individuals. For each participant, we extracted the maximum and minimum values of each of the three virtual waves; the constant component at the 101st is the virtual-wave offset value, and the static-frame amplitude at the 102nd data point, yielding 11 data points (the first component had no maximum peak, only a minimum). Polarity was fixed by multiplying each value by the sign of the corresponding image's mean. We also included an optional training parameter p: positive values indicate a patient with disease, negative values indicate a healthy individual, and zero indicates no training. We ran the simulation with different values, but present only $p=0$. We classified the extracted features using independent component analysis, a matrix factorization method for dimensionality reduction of the thermal data. We modeled the data as $\boldsymbol{X_i = A * S_i + N_i}$, where X_i denotes the observed data, $\boldsymbol{S}$ denotes the signal, $\boldsymbol{A}$ denotes the mixing matrix, and $\boldsymbol{N_i}$ denotes additive noise inherent in thermal acquisition [17]. We normalized each component across the entire ensemble. This normalization helps ensure that individual variance in physiological baseline does not disproportionately influence signature identification.

We used three vectors to construct $\boldsymbol{A}$. We applied the inverse of matrix $\boldsymbol{A}$ to each patient's data to generate a scatter plot after removing the component associated with the training data p. The resulting two clusters separate malignant and healthy cases even with $p = 0$ (unsupervised training), suggesting algorithmic robustness without training. Training appeared to have minimal effect on the final classification outcomes; the extracted thermal features have inherent discriminative power to distinguish between physiological conditions. Table one presents the resulting coefficients for unsupervised training.

	Primary predictor	2nd predictor	3rd predictor
Max 1st VW	2.0098	0.5879	-0.3796
Max 2nd VW	2.8165	0.0761	9.9348
Max 3rd VW	0.2357	-0.1564	-2.2120
Min 1st VW	-10.5295	-0.4327	-0.1841
Min 2nd VW	3.1047	-0.0487	-2.1089
Min 3rd VW	-0.0645	-8.3375	0.4096
Bias 1st VW	10.6931	0.5465	0.4871
Bias 2nd VW	-4.2946	-0.0003	-7.0323
Bias 3rd VW	2.1909	9.1731	0.2259
Static 1st	10.0314	0.3658	2.4252
Static 2nd	0.3308	-0.1353	9.3155
Static 3rd	1.2371	10.4612	0.0736

Table 1: Coefficients of the training results ($p = 0$, unsupervised) associated with: Virtual wave (VW); bias of the virtual wave; and the amplitude of the static frame.

The first predictor is dominated by the first component, followed by the second component. The third component dominates the second predictor, and the second component dominates the last predictor.



a First component of the ensemble analysis vs second component.

b First component of the ensemble analysis vs third component.

Figure 7 Scatter plot with no training (p = 0) indicates separation between pathological and non-pathological cohorts and supports the utility of independent component analysis for identifying diagnostic signatures.

4. **Discussion**

Initially, we aimed to characterize the vascular heat so we could remove it and identify the tumor's direct heat. However, this characterization proved to be a strong diagnostic tool based on thermo-regulatory responses. We still have to complete the original goal. Figure 7 provides the clearest evidence of this work's relevance; it was obtained using blindfold training, whereas healthy-or-sick classification was used only for the final display. Some patients classified as sick appear in the healthy group; this was expected because the data didn't indicate which breast was affected. A large number of healthy patients appear in the sick cluster; it is unclear whether the original DMR-IR study missed the cancer, our algorithm misdiagnosed, or the method identified precancerous lesions. This research marks a significant shift from conventional thermography, which addresses either static or dynamic thermograms alone. Earlier work incorporated physical thermal modeling through reverse modeling on static-only thermography data [16,17]. In a previous paper [5], we separated the basic physical heat response from physiological vasoconstriction using VWT. VWT is a physics-based inverse modeling approach. In this paper, we extend the approach to isolate relevant physiological variables and identify the cancer signature. However, we did not identify the exact physiological meaning. Further investigation may be warranted. The algorithm uses only the first two images, which are the hottest ones in the ICA signal. We interpret it as identifying the heat carried away from the tumor by the veins. The algorithm differs from deep learning models in two ways: first, artificial intelligence (AI) may provide an outcome without a clinically interpretable explanation (a "black box"). Second, the proposed algorithm may not require complete training; it operated without sick/healthy classification during training. The algorithm can be applied with a much smaller database and does not require prior complete, accurate medical characterization, which may be prohibitively costly.

The dataset includes only four patients with identified tumor locations; in one case, the image registration of the static image failed. Accordingly, conclusions based on three images may be unwarranted; additional data may be required to support more definitive inference. Future research may benefit from refining this approach by incorporating larger, histologically confirmed datasets, which may clarify whether these intermediate thermal signatures represent early-stage malignant markers or physiological noise. Furthermore, implementing sophisticated patient-specific numerical models could enable a transition from purely qualitative observations to quantitative assessments of these thermal phenomena [18]

5. Conclusion

The results suggest that dynamic thermography, when processed via independent component analysis, yields robust biomarkers for distinguishing malignant vascular signatures from healthy responses even when data quality is limited.

Appendix 1: DMR-IR database integrity

The study used publicly available breast cancer research data from DMR-IR, a Brazilian database [15], but acknowledged significant limitations due to insufficient clinical detail and incomplete information [19]. Key limitations included the scarcity of mammograms and biopsies, the broad patient classification limited to "sick" or "healthy" without specific diagnostic data, and the absence of laterality information. None of the patients underwent magnetic resonance imaging (MRI) or ultrasound [19]. Despite these limitations, it appears to be the only publicly available dataset containing both static and dynamic infrared data. As such, numerous papers have studied it. Because we analyzed each breast as an independent case, ambiguity in laterality appears to be a significant limitation, as the resulting sick-healthy classification does not distinguish laterality. However, because the training was blinded to sick-healthy data, this limitation had a negligible impact. Notably, considerable motion artifacts compromised many records, likely due to patient movement, as patients stood with no support. Static images, taken at separate times from the dynamic ones, further exacerbated motion artifacts. During the early study, a substantial subgroup of healthy patients appeared to exhibit thermal patterns that converged toward common statistical-behavioral clusters, potentially reflecting shared physiological variation in thermal regulation. Subsequent analysis identified that these thermographic signatures resulted from replacing static data with the first dynamic frame. The authors of the study should therefore submit a correction to the original paper acknowledging this error. This correction may be particularly warranted given the prevalence of this work in artificial intelligence breast cancer research.

Appendix 2: Image registration

Effective alignment between thermograms remains a critical challenge, as spatial discrepancies can introduce significant errors in subsequent thermal signature extraction [20]. Patients stood in front of the camera unsupported for five minutes. Some images suggest potential camera instability. Such misalignments require

image-registration algorithms to compensate for patient motion and sensor displacement, enabling accurate mapping of temporal dynamics across the breast surface. We implemented a two-stage registration procedure: first, we applied full-frame transformations using the MATLAB *imregister* function with the affine option, using the fifteenth frame as a reference, followed by manual segmentation to identify the region of interest (the breast). We then registered each breast separately using the same procedure. We registered the inner and outer regions separately, then stitched the resulting images. Because we only analyzed the ROI (the breast), we used the outer portion of the image only for display; the stitching process was not critical.

Appendix 3: Virtual wave transform

The virtual wave transform recast diffusive propagation as wave-like propagation [5, 21]. The transformation is based on the correspondence between the wave propagation equation, which contains a second-order time derivative, and the diffusion equation, which contains a first-order time derivative. In the discrete time domain, the transformation uses a matrix multiplication $\boldsymbol{W}$ that mirrors the temporal cooling profile.

$\boldsymbol{X_d} = \boldsymbol{X_w} * \boldsymbol{W}$ $\qquad W_{i,j} = exp(-\frac{\tau_i^2}{4\cdot(t_j+t_0)}) - exp(-\frac{\tau_i^2}{4\cdot t_j})$

VWT enables extraction of transient thermal components by mapping diffusive flow into a wave-like form. For virtual time, we used a logarithmic time scale :$\tau_j = 0.1 \cdot 2^{j/100}$ i = 1:100

. Although 100 points may exceed the minimum requirement, they appear to yield a clearer visual representation. For real-time, we used $t_i = 1{:}20$, corresponding to individual frames. This logarithmic discretization substantially reduces the computational burden of long-duration thermal sequences. The matrix $\boldsymbol{W}$ is highly singular and requires specialized handling. Accordingly, we apply a truncated singular value decomposition during inversion to ensure numerical stability and prevent noise from the source data from propagating. A modified truncated singular value decomposition was employed. Instead of using $1/\lambda_i$ and truncating the sequence at a certain value of *i*, we used $\lambda_i/({\lambda_i}^2 + \varepsilon{\lambda_0}^2)$ This modification appears to yield a smoother inversion with reduced ringing. We set. $\epsilon = 0.3$. When the data contain a constant temperature offset, the inversion may produce artifacts. We can mitigate these artifacts by including an extra column of $W_{101,\mathrm{j}} = 1$. This isolates the image's constant-temperature component in column 101 of the inverted data.

References

1. Wang, L. (2024). Mammography with deep learning for breast cancer detection. *Frontiers in Oncology*, *14*. https://doi.org/10.3389/fonc.2024.1281922

2. Ismail, H., Pretty, C. G., Signal, M., Haggers, M., & Chase, J. G. (2017). Attributes, Performance, and Gaps in Current & Emerging Breast Cancer Screening Technologies. *Current Medical Imaging Formerly Current Medical Imaging Reviews*, *15*(2), 122–131. https://doi.org/10.2174/1573405613666170825115032

3. Goñi-Arana, A., Pérez-Martín, J., & Díez, F. J. (2025). Why Do Radiologists Disown Breast Thermography? A Critical Review of Recent Studies and Recommendations. *Cancers*, *17*(13), 2195. https://doi.org/10.3390/cancers17132195

4. Arnold, M., Morgan, E., Rumgay, H., Costa, A. M. da, Singh, D., Laversanne, M., Vignat, J., Gralow, J. R., Cardoso, F., Siesling, S., & Soerjomataram, I. (2022). Current and future burden of breast cancer: Global statistics for 2020 and 2040. *The Breast*, *66*, 15–23. https://doi.org/10.1016/j.breast.2022.08.010

5. Gershenson, M., & Gershenson, J. (2023). Dynamic Vascular Imaging Using Active Breast Thermography. *Sensors*, *23*(6), 3012. https://doi.org/10.3390/s23063012

6. Szumiejko, A., Ptak, M., & Dołęga-Kozierowski, B. (2025). Computational Methods in Breast Cancer Diagnostics and Surgery Planning: A Review. *Archives of Computational Methods in Engineering*. https://doi.org/10.1007/s11831-025-10410-9

7. Anbar, M. (1995). <title>Dynamic area telethermometry and its clinical applications</title>. *Proceedings of SPIE, the International Society for Optical Engineering/Proceedings of SPIE*, *2473*, 312–322. https://doi.org/10.1117/12.204868

8. Moraes, M. F. B., Сфаppa, C., Fernandes, H., & Figueiredo, A. (2025). Influence of thermal contrast and limitations of a deep-learning based estimation of early-stage tumour parameters in different breast shapes using simulated passive and dynamic thermography. *Thermal Science and Engineering Progress*, *60*, 103418. https://doi.org/10.1016/j.tsep.2025.103418

9. Barba, D., León-Sosa, A., Lugo, P., Suquillo, D., Torres, F., Surre, F., Trojman, L., & Caicedo, A. (2020). Breast cancer, screening and diagnostic tools: All you need to know [Review of *Breast cancer, screening and diagnostic tools: All you need to know*]. *Critical Reviews in Oncology/Hematology*, *157*, 103174. Elsevier BV. https://doi.org/10.1016/j.critrevonc.2020.103174

10. Kakileti, S. T., Manjunath, G., Madhu, H., & Ramprakash, H. V. (2017). Advances in Breast Thermography. In *InTech eBooks*. https://doi.org/10.5772/intechopen.69198

11 Karanam, P. K., Kompella, S., Chittineni, S., Nadamuni, V. S. D., & Anna, S. (2025). Constraint-Embedded Deep Learning for Breast Cancer Diagnosis Using Thermogram Images: An Experimental Study. *Premier Journal of Science.* https://doi.org/10.70389/pjs.100130

12. Ciardiello, A., D'Angelo, A., Angelis, L. D., Giagu, S., Sala, E., & Gigante, G. (2026). Beyond the black box: lessons in explainability from AI in mammography. *Artificial Intelligence Review*. https://doi.org/10.1007/s10462-026-11518-5

13. Yousefi, B., Hershman, M., Fernandes, H., & Maldague, X. (2021). *Concentrated Thermomics for Early Diagnosis of Breast Cancer*. 30. https://doi.org/10.3390/engproc2021008030

14. Ramaswamy, R., Joseph, E. R., & Muthukumaraswamy, S. A. (2026). Thermal diffusion–based subsurface Depth Estimation in Active Infrared Thermography Using Thermal Signal Reconstruction and Deep Learning. In *Research Square*. https://doi.org/10.21203/rs.3.rs-8503061/v1

15. Silva, L. F., Saade, D. C. M., Sequeiros, G. O., Silva, A. C., Paiva, A. C. de, Bravo, R., & Conci, A. (2013). A New Database for Breast Research with Infrared Image. *Journal of Medical Imaging and Health Informatics*, *4*(1), 92–100. https://doi.org/10.1166/jmihi.2014.1226

16. Perez-Raya, I., Gutiérrez, C., & Kandlikar, S. G. (2024). A Transformative Approach for Breast Cancer Detection Using Physics-Informed Neural Network and Surface Temperature Data. *ASME Journal of Heat and Mass Transfer*, *146*(10). https://doi.org/10.1115/1.4065673

17. . Sritharan, N., Gutiérrez, C., Perez-Raya, I., Gonzalez-Hernandez, J.-L., Owens, A., Dabydeen, D., Medeiros, L., Kandlikar, S. G., & Phatak, P. D. (2024). Breast Cancer Screening Using Inverse Modeling of Surface

Temperatures and Steady-State Thermal Imaging. *Cancers*, *16*(12), 2264. https://doi.org/10.3390/cancers16122264 26. Agostini, V., Ala, A., Bussone, R., Ciarlini, A. E. M.,

18. Mukhmetov, O., Igali, D., Zhao, Y., Ng, E. Y. K., Fok, S. C., & Teh, S. L. (2021). Thermal modeling for breast tumor detection using thermography. *International Journal of Thermal Sciences*, *161*, 106712. https://doi.org/10.1016/j.ijthermalsci.2020.106712

19. Pérez-Martín, J., & Sánchez-Cauce, R. (2023). Quality analysis of a breast thermal images database. *Health Informatics Journal*, *29*(1). https://doi.org/10.1177/14604582231153779

20. V. Agostini, S. Delsanto, M. Knaflitz and F. Molinari, "Noise Estimation in Infrared Image Sequences: A Tool for the Quantitative Evaluation of the Effectiveness of Registration Algorithms," in *IEEE Transactions on Biomedical Engineering*, vol. 55, no. 7, pp. 1917-1920, July 2008, doi: 10.1109/TBME.2008.919842

21. Kovács, P., Lehner, B., Thummerer, G., Mayr, G., Burgholzer, P., & Huemer, M. (2021). Surfing Virtual Waves to Thermal Tomography: From model- to deep learning-based reconstructions. *IEEE Signal Processing Magazine*, *39*(1), 55–67. https://doi.org/10.1109/msp.2021.3120978

Funding: This research received no external funding.

Informed Consent Statement: Not applicable.

Data Availability Statement: http://visual.ic.uff.br/dmi [Accessed October 27, 2026]

Conflicts of Interest: The authors declare no conflicts of interest.

Acknowledgment: Thanks to Jonathan Gershenson for the useful discussions